Check for updates

The self-assembly of a pair of low-symmetry tetracarboxylic acid molecules and their co-assembly with bridging molecules at the liquid–solid interface†

Siqi Zhang,[a,b] Jianqiao Li,[b] Linlin Gan,[b] Lin Ma,[b] Wei Ma,[d] Min Zhang,*[a] Faliang Cheng,*[a] Ke Deng 🔾 *[b] and Qingdao Zeng 🔾 *[b,c]

The supramolecular self-assembly behavior of a pair of low-symmetry tetracarboxylic acid molecules (H_4OBDB and H_4ADDI) and their co-assembly behavior with TMA as a bridging molecule were studied at the liquid–solid interface. Scanning tunneling microscope (STM) observations revealed that H_4OBDB and H_4ADDI molecules both tend to form O-shaped dimers but end up forming different types of self-assembly structures. We also investigated the construction of two-component co-assembly structures by mixing H_4OBDB or H_4ADDI molecules with bridging molecules such as TMA. The two formed co-assembly structures are similar. Based on the analysis of the STM results and the density functional theory (DFT) calculations, the formation mechanism of the assembled structures was revealed.

[a]*Guangdong Engineering and Technology Research Center for Advanced Nanomaterials, School of Environment and Civil Engineering, Dongguan University of Technology, Dongguan 523808, China. E-mail: mindear@dgut.edu.cn, chengfl@dgut.edu.cn*
[b]*CAS Key Laboratory of Standardization and Measurement for Nanotechnology, CAS Center for Excellence in Nanoscience, National Center for Nanoscience and Technology (NCNST), Beijing 100190, China. E-mail: kdeng@nanoctr.cn, zenqd@nanoctr.cn*
[c]*Center of Materials Science and Optoelectronics Engineering, University of Chinese Academy of Sciences, Beijing 100049, China*
[d]*State Key Laboratory for Mechanical Behavior of Materials, Xi'an Jiaotong University, Xi'an 710049, China*
†Electronic supplementary information (ESI) available: DFT-simulated single molecular models on the graphite surface and details of DFT-simulated molecular models of all assembled structures. See DOI: https://doi.org/10.1039/d2nr06740d

Introduction

Supramolecular self-assembly is an impeccable system in the natural world for spontaneously forming well-organized materials, such as cellular membranes.[1,2] Over the past few decades, many researchers have learned from nature and devoted themselves to the design and construction of complex functional supramolecular structures using simple molecular building blocks.[3–7] The systematic study of molecular self-assembly is beneficial for simulating its properties in the designation of functional nanomaterials and devices. The key to obtaining a deep understanding of self-assembly is molecular-level research of the specific assembly system. Scanning tunneling microscopy (STM) is a powerful tool to characterize two-dimensional supramolecular assemblies with submolecular resolution.[8–10] The liquid–solid interface between the molecular solution and the solid surface of highly oriented pyrolitic graphite (HOPG) provides an ideal planar solid substrate for supramolecular self-assembly and an environment for studying the dynamic process of molecular self-assembly under the synergistic effects of various driving forces in the system. Extensive STM investigations have been conducted at the liquid–solid interface in recent years.[11–19]

Among the intermolecular noncovalent driving forces of molecular self-assembly, hydrogen bonding is the strongest and therefore one of the most important methodologies for preparing supramolecular structures. In addition, the selectivity and directivity of hydrogen bonds are noteworthy aspects concerning molecular self-assembly, and the self-assembly structures driven by the hydrogen bonds are more predictable and controllable.[20–26] In particular, cyclic dimeric O–H···O hydrogen bonds between two carboxyl groups have been widely used in the construction of particular 2D supramolecular architectures at the liquid–solid interface.[27–31] For instance, with the dimeric hydrogen bonds between carboxyl groups as the main driving force of self-assembly, trimesic acid (TMA) molecules can form a typical honeycomb network structure;[32–34] tetracarboxylic acid molecules such as NN4A and H_4ETTC can form a Kagomé or a quadrilateral network

structure, respectively;[35,36] flexible carboxylic porphyrin derivative IPETPP containing eight carboxyl groups can form both Kagomé and quadrilateral network structures.[37]

The position of the carboxyl groups at the molecule core determines whether long-range ordered structures can be observed.[38,39] A bonding angle of 180° between carboxylic groups of adjacent molecules is ideal, which enables the molecules to be arranged into a relatively strong and highly predictable network structure.[40] In general, structures stabilized by dimeric hydrogen bonds between carboxyl groups, which have well-ordered symmetrical geometries, were constructed using molecular building blocks that have a symmetrical distribution of carboxyl groups. In this case, C_3-symmetric aromatic tricarboxylic/hexacarboxylic acids and D_{2h}-symmetric aromatic tetracarboxylic acids are common building block choices. To enrich the topology of the assembled structure, it is of considerable interest to impose structural variations on a well-studied molecule type such as C_3-symmetric tricarboxylic acid. For example, with a larger core size than TMA, C_3-symmetric 1,3,5-benzenetribenzoic acid (BTB) tends to form a densely packed structure with a rectangular cavity rather than a hexagonal honeycomb structure that comprises weaker C–H⋯O bonds but increases molecular packing.[41] When the symmetry of the building block is reduced, the assembled structure becomes less predictable, yet it opens up an opportunity to access a variety of possible structures. Although systematic studies are lacking, some self-assembly studies of low-symmetry building blocks have been carried out in recent years.[42–44] Morrison *et al.* reduced the symmetry of BTB by changing the sites of carboxyl groups and the assembly structure was significantly diversified.[45] Wang *et al.* observed two kinds of self-assembly of C_{2v}-symmetric tetracarboxylic acid (TPTA).[46] In our previous study, a low-symmetry pentacarboxylic acid (H₅BHB) that participated in co-assembly with pyridine molecules using its C_2-symmetric dimer as the basic building block was reported.[47]

In this article, we report the self-assembly of a pair of low-symmetry tetracarboxylic acid molecules (H₄OBDB and H₄ADDI) at the heptanoic acid solvent solution–HOPG liquid–solid interface. As shown in Scheme 1, H₄OBDB and H₄ADDI are similar in structure, both having a semicircular bent skeleton and an isophthalic acid group at two ends of the skeleton. The difference is that H₄OBDB incorporates a diphenyl ether group, whereas H₄ADDI contains an acridine group. Due to the rotation of C–O bonds, H₄OBDB will be more flexible than the rigid H₄ADDI molecule. Their synthesis procedures have been reported in the previous literature.[48,49] Comparing the similarities and differences of their self-assembly behaviors will provide an understanding of how the different assembly factors are related to each other, with the key point being developing a diverse topology of assembly structures and greater sophistication in predicting self-assembly architectures using low-symmetry building blocks. We also investigated the construction of two-component co-assembly structures by mixing H₄OBDB or H₄ADDI molecules with bridging molecules such as TMA. Through STM observations and density
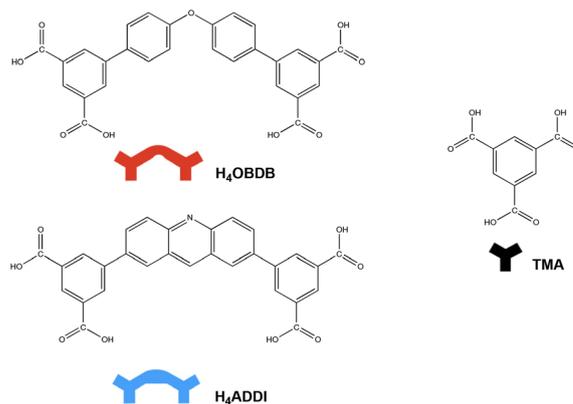
**Scheme 1** Chemical structures of 4′,4‴-oxybis[1,1′-biphenyl]-3,5-dicarboxylic acid (H₄OBDB), 5,5′-(acridine-2,7-diyl)diisophthalic acid (H₄ADDI), and trimesic acid (TMA).

functional theory (DFT) calculations, the formation mechanism of the assembled structures was revealed.

Results and discussion

Self-assembly of H₄OBDB at the liquid–solid interface

4′,4‴-Oxybis[1,1′-biphenyl]-3,5-dicarboxylic acid (H₄OBDB) is a semi-rigid bent-shaped molecule with a diphenyl ether group in the middle of the skeleton and an isophthalic acid group at each terminal. After depositing a droplet of H₄OBDB heptanoic acid solvent solution on a freshly cleaved HOPG surface, a dense and well-ordered monolayer was formed immediately at the liquid–solid interface at room temperature. It can be seen from the STM image in Fig. 1a and b that the H₄OBDB molecule assembled into two different types of patterns, which were marked by stru1 and stru2, respectively. In type stru1, the H₄OBDB self-assembly structure is densely packed and exhibits a linear motif (denoted as H₄OBDB_stru1), while in type stru2, the H₄OBDB self-assembly structure is loosely arranged and exhibits a hexagonal symmetric motif (denoted as H₄OBDB_stru2). The small-scale STM images of H₄OBDB_stru1 and H₄OBDB_stru2 with distinct molecular resolutions are shown in Fig. 1c and d, respectively. A careful analysis of these two assembled structures provides us with a preliminary understanding of the self-assembly behavior of the H₄OBDB molecule. In Fig. 1c, the X-shaped highlighted contour is consistent with the skeleton of two neighboring H₄OBDB molecules arranged "back to back", whereas in Fig. 1d, the O-shaped highlighted contour agrees with the skeleton of two neighboring H₄OBDB molecules arranged "face to face". From the location of the hydrogen bond donor and acceptor moieties on its semicircular skeleton, it is not difficult to infer that two H₄OBDB molecules can form double cyclic dimeric O–H⋯O hydrogen bonds between their carboxyl groups, thus forming an O-shaped dimer. At the same time, the central oxygen atom of the H₄OBDB molecule can also form an O⋯H–C hydrogen bond with the hydrogen atom on
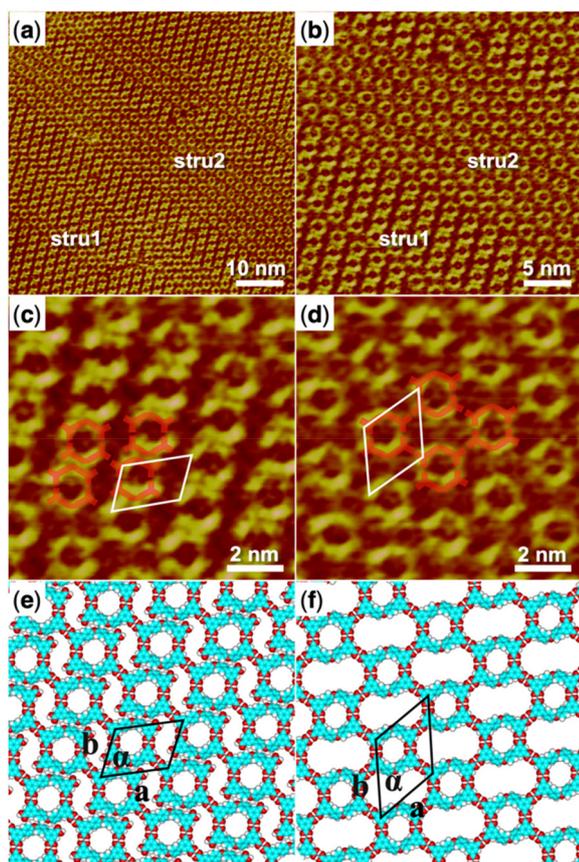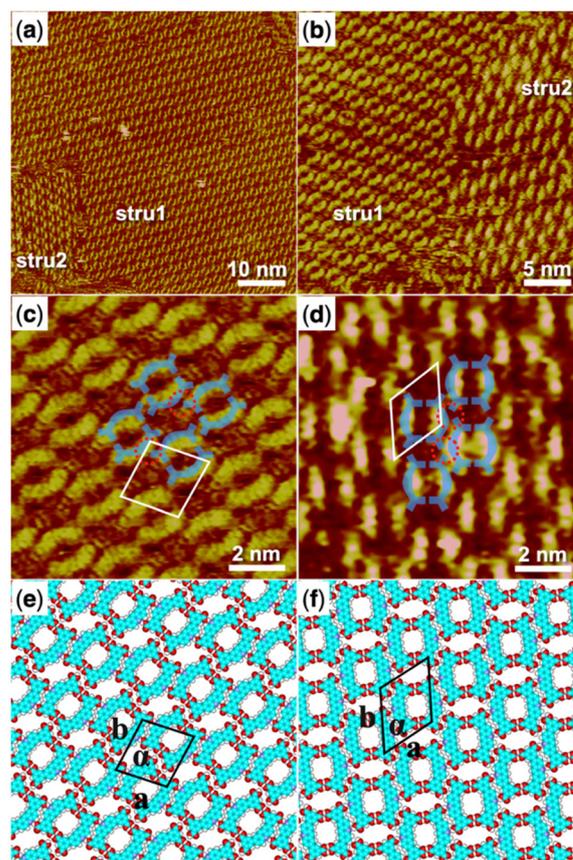
Fig. 1 (a) STM image (60 nm × 60 nm) of H_4OBDB self-assembly at the heptanoic acid–HOPG liquid–solid interface, I_{set} = 299.1 pA, V_{bias} = 699.8 mV. (b) STM image (30 nm × 30 nm) of H_4OBDB self-assembly, I_{set} = 299.1 pA, V_{bias} = 699.8 mV. (c) High-resolution STM image (10 nm × 10 nm) of H_4OBDB_stru1, I_{set} = 299.1 pA, V_{bias} = 699.8 mV. (d) High-resolution STM image (10 nm × 10 nm) of H_4OBDB_stru2, I_{set} = 299.1 pA, V_{bias} = 699.8 mV. (e) Suggested molecular model for H_4OBDB_stru1. (f) Suggested molecular model for H_4OBDB_stru2. Unit cells were imposed on the STM image and its molecular model. Their measured and calculated parameters are shown in Table 1.

form a porous network structure. Further analysis of the thermodynamic stability of these two self-assembly structures will be conducted in combination with DFT-calculated data.

Self-assembly of H_4ADDI at the liquid–solid interface

5,5′-(Acridine-2,7-diyl)diisophthalic acid (H_4ADDI) is also a bent-shaped tetracarboxylic molecule similar to H_4OBDB, but with an acridine group in the middle of the skeleton. Two types of well-ordered self-assembly monolayers were formed as observed in large-scale STM images of Fig. 2a and b after depositing a droplet of heptanoic acid solution containing H_4ADDI on the surface of the HOPG substrate, which was marked by stru1 and stru2. In type stru1, an alignment pattern of distinct O-shaped dimers was observed (denoted as H_4ADDI_stru1). Compared with type stru1, type stru2 is arranged in a hexagonal symmetric pattern (denoted as H_4ADDI_stru2) and has a lower proportion on the substrate.
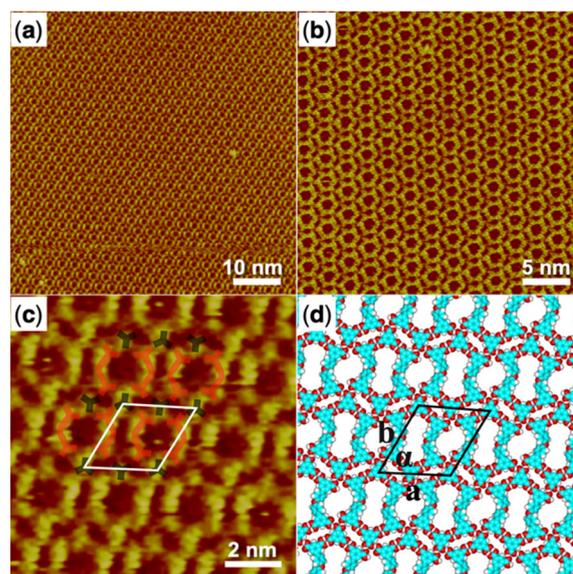

Fig. 2 (a) STM image (60 nm × 60 nm) of H_4ADDI self-assembly at the heptanoic acid–HOPG liquid–solid interface, I_{set} = 140.4 pA, V_{bias} = 923.5 mV. (b) STM image (30 nm × 30 nm) of H_4ADDI self-assembly, I_{set} = 283.8 pA, V_{bias} = 661.0 mV. (c) High-resolution STM image (10 nm × 10 nm) of H_4ADDI_stru1, I_{set} = 283.8 pA, V_{bias} = 661.0 mV. (d) High-resolution STM image (10 nm × 10 nm) of H_4ADDI_stru2, I_{set} = 140.4 pA, V_{bias} = 923.5 mV. (e) Suggested molecular model for H_4ADDI_stru1. (f) Suggested molecular model for H_4ADDI_stru2. Unit cells were imposed on the STM image and its molecular model. Their measured and calculated parameters are shown in Table 1.

its skeleton, allowing two H_4OBDB molecules to appear as an X-shaped dimeric contour. Fig. 1e and f show the corresponding molecular models optimized by the DFT method based on the STM observation of H_4OBDB_stru1 and H_4OBDB_stru2, respectively. The molecular model is consistent with the STM images in terms of adsorbate geometry and unit cell parameters. It can clearly be seen that, in H_4OBDB_stru1, H_4OBDB molecules can form O-shaped dimers and are simultaneously attached by hydrogen bonds between diphenyl ether groups; in this case, the O-shaped dimers are stacked parallel to each other in columns. Three of the four carboxyl groups of the H_4OBDB molecule bond with carboxyl groups of adjacent H_4OBDB molecules, and the other one can also form an O···H–C hydrogen bond with the hydrogen atom on the benzene ring. In H_4OBDB_stru2, only O-shaped dimers of the H_4OBDB molecule appear and they are connected by hydrogen bonds between carboxyl groups to

High-resolution STM images of H$_4$ADDI_stru1 and H$_4$ADDI_stru2 are shown in Fig. 2c and d, respectively. Although H$_4$ADDI has a similar structure to H$_4$OBDB, its assembly strategy is different from that of H$_4$OBDB. Undoubtedly, the O-shaped contour in Fig. 2c corresponds to the dimer of H$_4$ADDI formed by the double cyclic dimeric O–H⋯O hydrogen bonds between terminal carboxyl groups. As illustrated by the imposed blue-coloured symbol representing the H$_4$ADDI molecule, the X-shaped dimer of H$_4$ADDI does not occur, but a vacancy terminal carboxyl group of the H$_4$ADDI molecule is observed to be close to the middle moiety of an adjacent H$_4$ADDI molecule (as shown in the red dashed circles in Fig. 2c), forming a misplaced X-type linkage, and then the O-shaped dimers are assembled into H$_4$ADDI_stru1. In Fig. 2d, the middle moiety of the H$_4$ADDI molecule is attached to carboxyl groups of two adjacent molecules (as shown in the red dashed circles in Fig. 2d), which increases the molecular packing of the assembled H$_4$ADDI_stru2. Fig. 2e and f show the corresponding molecular models optimized by the DFT method based on the STM observation of H$_4$ADDI_stru1 and H$_4$ADDI_stru2, respectively. As shown in the molecular models, N⋯H–O and O⋯H–C hydrogen bonds could be formed between the acridine group and the terminal carboxyl group of neighboring H$_4$ADDI molecules. In H$_4$ADDI_stru1, an acridine group is connected to a carboxyl group by a N⋯H–O hydrogen bond, while in H$_4$ADDI_stru2, an acridine group is connected to a carboxyl group by a N⋯H–O hydrogen bond and to a second carboxyl group by a C–H⋯O hydrogen bond. The molecular models are in good agreement with the STM images. Further analysis of the thermodynamic stability of these two self-assembly structures will be conducted in combination with the DFT data in the following section.

Co-assembly of H$_4$OBDB and TMA at the liquid–solid interface

We then started to investigate the trimesic acid (TMA) molecule as a bridging molecule to expand the self-assembly network of the H$_4$OBDB molecule. When a droplet of heptanoic acid solution containing H$_4$OBDB and TMA was added to the surface of HOPG, we observed that the assembled monolayer structure (denoted as H$_4$OBDB–TMA) covers the entire surface immediately, as shown in the large-scale STM image in Fig. 3a and b. In the high-resolution STM image of Fig. 3c, it can be clearly seen that the dot-shaped structure representing the TMA molecule and the long bar-shaped structure representing the H$_4$OBDB molecule mixed to form a porous hexagonal co-assembly pattern. Fig. 3d shows the corresponding DFT-optimized molecular model of H$_4$OBDB–TMA. The unit cell parameters of the DFT model were in good agreement with those measured in the STM image, indicating that the model is reasonable. Two of the three carboxyl groups of each TMA molecule form cyclic dimeric O–H⋯O hydrogen bonds with two adjacent H$_4$OBDB molecules and the other one can form two O–H⋯O hydrogen bonds with the other two adjacent H$_4$OBDB molecules. Two H$_4$OBDB molecules and two TMA molecules form the minimal repeated building block of the
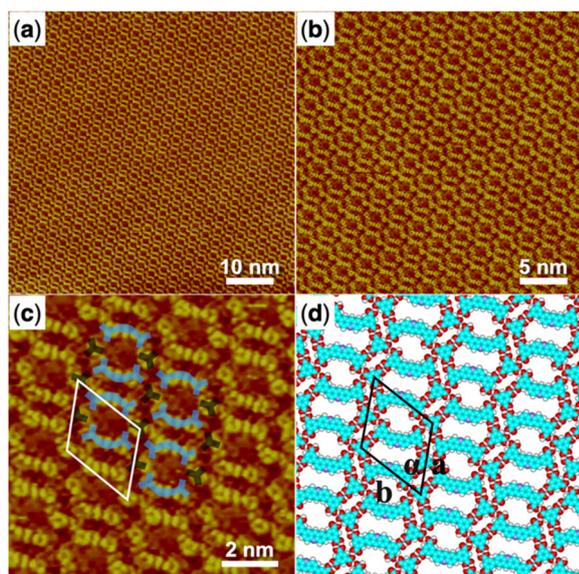

Fig. 3 (a) STM image (60 nm × 60 nm) of H$_4$OBDB–TMA co-assembly at the heptanoic acid–HOPG liquid–solid interface, I_{set} = 228.9 pA, V_{bias} = 693.1 mV. (b) STM image (30 nm × 30 nm) of H$_4$OBDB–TMA co-assembly, I_{set} = 296.0 pA, V_{bias} = 698.9 mV. (c) High-resolution STM image (10 nm × 10 nm) of H$_4$OBDB–TMA co-assembly, I_{set} = 228.9 pA, V_{bias} = 693.1 mV. (d) Suggested molecular model for H$_4$OBDB–TMA co-assembly. Unit cells were imposed on the STM image and its molecular model. Their measured and calculated parameters are shown in Table 1.

H$_4$OBDB–TMA co-assembly structure, which is then spliced into a large range of an ordered pattern. The ratio of the H$_4$OBDB molecule to the TMA molecule is 1 : 1 in the co-assembly structure. With a periodic arrangement of nano-cavities of different sizes, the co-assembly structure can be further studied in the field of selective molecular recognition.

Co-assembly of H$_4$ADDI and TMA at the liquid–solid interface

The co-assembly of the H$_4$ADDI molecule and the TMA molecule was also carried out and the large-scale STM image of the obtained H$_4$ADDI–TMA co-assembly monolayer structure is shown in Fig. 4a and b. It can be observed that the H$_4$ADDI–TMA structure is similar to the H$_4$OBDB–TMA structure. In the high-resolution STM image in Fig. 4b, we can see that the TMA molecule appears as a dot-shaped structure and the H$_4$ADDI molecule appears as a bar-shaped structure. Fig. 4d shows the corresponding molecular model of H$_4$ADDI–TMA, which was based on the STM observation and optimized by the DFT method. The interactions between the molecules are quite clear, and the molecular model matches the STM image well. A TMA molecule also forms two cyclic dimeric O–H⋯O hydrogen bonds with two adjacent H$_4$ADDI molecules and two O–H⋯O hydrogen bonds with the other two adjacent H$_4$OBDB molecules. The ratio of the H$_4$ ADDI molecule to the TMA molecule is also 1 : 1 in the co-assembly structure.

In conclusion, the self-assembly behavior of a pair of low-symmetry carboxylic acid molecules (H$_4$OBDB and H$_4$ADDI) and the co-assembly behavior of bridging molecules such as

Fig. 4 (a) STM image (60 nm × 60 nm) of H₄ADDI–TMA co-assembly at the heptanoic acid–HOPG liquid–solid interface, I_{set} = 289.9 pA, V_{bias} = 727.5 mV. (b) STM image (30 nm × 30 nm) of H₄ADDI–TMA co-assembly, I_{set} = 289.9 pA, V_{bias} = 727.5 mV. (c) High-resolution STM image (10 nm × 10 nm) of H₄ADDI–TMA co-assembly, I_{set} = 289.9 pA, V_{bias} = 727.5 mV. (d) Suggested molecular model for H₄ADDI–TMA co-assembly. Unit cells are imposed on the STM image and its molecular model. Their measured and calculated parameters are shown in Table 1.

TMA were studied. H₄OBDB and H₄ADDI molecules have similar semicircular bent-shaped structures and both tend to form an O-shaped dimer *via* strong intermolecular double cyclic dimeric O–H⋯O hydrogen bonds between terminal carboxyl groups, but end up forming different monolayer self-assembly structures at the liquid–solid interface. The configurations of the self-assembled structures are determined by the connections between the O-shaped dimers. In addition to the cyclic dimeric O–H⋯O hydrogen bonds between carboxyl groups, for the H₄OBDB molecule, the double O⋯H–C hydrogen bonds between diphenyl ether groups are also considerable driving forces for its self-assembly. For the H₄ADDI molecule, its acridine group can connect to adjacent vacant carboxyl groups by a N⋯H–O hydrogen bond and a C–H⋯O hydrogen bond, which has an important impact on its self-assembly. After mixing with the TMA molecule, both H₄OBDB and H₄ADDI can form a precise arrangement of co-assembly with TMA through hydrogen bonding. The two co-assembly structures are similar because four terminal carboxyl groups of the tetracarboxylic molecule are all connected to the TMA bridging molecule by O–H⋯O hydrogen bonds, and thus the influence of different skeleton moieties on the co-assembly structure is limited.

Density functional theory (DFT) calculation results

To further reveal the formation mechanism of each assembled orderly structure at the liquid–solid interface from a theore-

tical perspective, we performed DFT calculations based on the above observed STM experimental results.

The measured and calculated unit cell parameters for all assembled structures are summarized in Table 1. The calculated parameters agree well with the experimental data, indicating that our DFT results are reasonable. In the surface assembly system, the interaction between adsorbates and the substrate plays an important role. Therefore, we present the total energy (including the interaction energy between adsorbates and the interaction energy between adsorbates and the substrate) in Table 2. Furthermore, a reasonable way to compare the thermodynamic stability of differently assembled structures should be the total energy per unit area. Hence, we also present the total energy per unit areas of the assembled structures in Table 2.

In Table 2, we noticed that H₄OBDB_stru1 had a lower total energy per unit area (−0.385 kcal mol⁻¹ Å⁻²) than H₄OBDB_stru2 (−0.330 kcal mol⁻¹ Å⁻²). This means that H₄OBDB_stru1 has higher thermodynamic stability than

Table 1 Experimental (Expt.) and calculated (Cal.) unit cell parameters for the assembled structures

		Unit cell parameters		
		a (nm)	b (nm)	α (°)
H₄OBDB_stru1	Expt.	2.5 ± 0.1	1.9 ± 0.1	67 ± 1
	Cal.	2.50	1.90	66.7
H₄OBDB_stru2	Expt.	2.4 ± 0.1	2.8 ± 0.1	55 ± 1
	Cal.	2.45	2.90	55.0
H₄ADDI_stru1	Expt.	2.1 ± 0.1	2.2 ± 0.1	79 ± 1
	Cal.	2.05	2.15	79.5
H₄ADDI_stru2	Expt.	2.0 ± 0.1	2.4 ± 0.1	60 ± 1
	Cal.	2.10	2.40	60.0
H₄OBDB–TMA	Expt.	2.6 ± 0.1	2.7 ± 0.1	63 ± 1
	Cal.	2.60	2.75	63.0
H₄ADDI–TMA	Expt.	2.6 ± 0.1	2.7 ± 0.1	61 ± 1
	Cal.	2.65	2.75	61.0

Table 2 The total energy (including the interaction energy between adsorbates and the interaction energy between adsorbates and the substrate) and energy per unit area for adsorbates on the HOPG surface. Here, the more negative energy means the system is more stable

	Interactions between molecules (kcal mol⁻¹)	Interactions between molecules and substrate (kcal mol⁻¹)	Total energy (kcal mol⁻¹)	Energy per unit area (kcal mol⁻¹ Å⁻²)
H₄OBDB_stru1	−95.030	−73.116	−168.146	−0.385
H₄OBDB_stru2	−116.215	−76.067	−192.282	−0.330
H₄ADDI_stru1	−82.396	−103.266	−185.662	−0.428
H₄ADDI_stru2	−81.366	−104.063	−185.429	−0.425
H₄OBDB–TMA	−141.138	−115.554	−256.692	−0.403
H₄ADDI–TMA	−127.224	−154.624	−281.848	−0.442

H$_4$OBDB_stru2. This is due to the high molecular density of H$_4$OBDB_stru1 and the strong hydrogen bond interactions between diphenyl ether groups of adjacent H$_4$OBDB molecules. In the experiment, it was observed that H$_4$OBDB_stru1 occupies a large domain area on the substrate and H$_4$OBDB_stru2 only appears at the domain boundary, which is consistent with the thermodynamic theoretical results. As for H$_4$ADDI_stru1 and H$_4$ADDI_stru2, the values for total energy per unit area are −0.428 kcal mol^{-1} Å^{-2} and −0.425 kcal mol^{-1} Å^{-2}, respectively. The theoretical result suggests that H$_4$ADDI_stru1 and H$_4$ADDI_stru2 have similar thermodynamic stabilities. In the experiment, it was also observed that H$_4$ADDI_stru1 has a higher proportion on the substrate, meaning that there is competition between kinetic factors occurring in the self-assembly of the H$_4$ADDI molecule, and the formation of H$_4$ADDI_stru1 is a kinetic priority. According to the DFT-simulated single molecular models in Fig. S1 in the ESI,† the H$_4$ADDI molecule has better planarity than H$_4$OBDB on the graphite substrate and therefore has a stronger π–π stacking interaction with the substrate, which is reflected by the corresponding data in Table 2.

It is noteworthy that the values of the total energy per unit area of H$_4$OBDB–TMA and H$_4$ADDI–TMA co-assembly structures are lower than those of the H$_4$OBDB and H$_4$ADDI self-assembly structures, revealing that the two co-assembly structures are more thermodynamically stable than the self-assembly structures. This means that, from a thermodynamics perspective, the structural transformation from the self-assembly structure to two-component co-assembly structures could occur by adding TMA molecules, which is consistent with the experimental results. In general, all the DFT calculation results agreed well with the STM observations and were self-consistent. The STM observation combined with DFT calculations illustrated how different assembly driving forces, such as molecule–molecule interactions and molecule–substrate interactions, synergistically influence the formation process and structure of the assembled monolayers on the surface. In this study, the molecule–molecule interactions mainly refer to different hydrogen bonds, and the spatial shape of the molecules and the position of the hydrogen bond groups on the molecular skeleton determine the assembled structures in the long range.

Experimental methods

STM investigation

All commercial reagents were used as received without further purification. Heptanoic acid solvent was purchased from Aldrich. H$_4$OBDB, H$_4$ADDI, and TMA molecules were purchased from Jilin Chinese Academy of Sciences—Yanshen Technology Co., Ltd (chemical structures are shown in Scheme 1). The solutions for the STM experiment were obtained by dissolving the molecules in heptanoic acid solvent. Unless otherwise noted, all solutions had a concentration of around 1.0 × 10^{-4} M. Specifically, all solutions were diluted to 10% of the saturated concentration because their typical saturated concentrations were generally 1.0 × 10^{-3} M. Highly oriented pyrolytic graphite (HOPG, grade ZYB, NTMDT, Russia) was used as the substrate and was cleaved using adhesive tape. The STM samples were prepared by depositing a droplet (0.4 µL) of solution onto the bare surface of the freshly cleaved HOPG substrate. After the treatments, STM experiments were performed with a Nanoscope III scanning probe microscope system (Bruker, USA) operating in a constant current mode under ambient conditions. An STM probe tip was prepared by mechanically cutting Pt/Ir wire (80/20) and immersed in the deposited solution during imaging. The provided STM images are raw data without any treatment except for the flattening process. The detailed tunneling conditions are given in the corresponding figure captions.

Computational details

The theoretical calculations were carried out using density functional theory (DFT) provided by the DMol^3 code.[50] We used the periodic boundary conditions (PBC) to describe the 2D periodic structure on the graphite in this work. The Perdew and Wang parameterization of the local exchange–correlation energy was applied in the local spin density approximation (LSDA) to describe exchange and correlation.[51,52] All-electron spin-unrestricted Kohn–Sham wave functions were expanded on a local atomic orbital basis. A numerical basis set was applied for the large system. The calculations were equipped with the medium mesh and were all-electron ones. The self-consistent field procedure was performed with a convergence criterion of 10^{-5} a.u. on the energy and electron density. Combined with the experimental data, we optimized the unit cell parameters and the geometry of the adsorbates in the unit cell. When the energy and density convergence criteria reached the desired degree, we could obtain the optimized parameters and the interaction energy between adsorbates.

The model system shows the interactions between the adsorbates and HOPG. In this investigation, the adsorption of adsorbates with a π-conjugated benzene-ring on graphite is similar to that of graphene, which helps us to perform calculations on infinite graphene monolayers using PBC. Graphene layers were separated by 40 Å in the normal direction. Graphene supercells were used and the Brillouin zone was sampled using a gamma point mesh when adsorbates were modeled on graphene. The interaction energy (E_{inter}) of adsorbates on graphite is $E_{inter} = E_{tot(adsorbates/graphene)} - E_{tot(isolated\ adsorbates\ in\ vacuum)} - E_{tot(graphene)}$.

Conclusions

In summary, the supramolecular self-assembly behavior of a pair of low-symmetry carboxylic acid molecules (H$_4$OBDB and H$_4$ADDI) and their co-assembly behaviors with a TMA bridging molecule were studied at the heptanoic acid–HOPG liquid–solid interface using an STM in combination with DFT calculations. H$_4$OBDB and H$_4$ADDI molecules both tend to form an

O-shaped dimer *via* intermolecular double cyclic dimeric O–H⋯O hydrogen bonds between terminal carboxyl groups but end up forming different types of self-assembly structures. The connections between the O-shaped dimers in different self-assembly structures were investigated and discussed. We also investigated the construction of two-component co-assembly structures by mixing H_4OBDB or H_4ADDI molecules with bridging molecules such as TMA. The two formed co-assembly structures are similar, suggesting that the influence of different skeleton moieties on the co-assembly structure is limited. The present work demonstrates how different assembly factors are related to each other, which has some implications for the chemical structural design of low-symmetry carboxylic acid molecules and the selection of other bridging molecules in future on-surface self-assembly studies. Based on the analysis of the STM results and the DFT calculations, the mechanisms of assembly behaviors were explored.

Conflicts of interest

There are no conflicts to declare.

Acknowledgements

References

1 D. Philp and J. F. Stoddart, *Angew. Chem., Int. Ed. Engl.*, 1996, **35**, 1154–1196.

2 G. M. Whitesides and B. Grzybowski, *Science*, 2002, **295**, 2418–2421.

3 J. A. Theobald, N. S. Oxtoby, M. A. Phillips, N. R. Champness and P. H. Beton, *Nature*, 2003, **424**, 1029–1031.

4 J. A. A. W. Elemans, S. Lei and S. De Feyter, *Angew. Chem., Int. Ed.*, 2009, **48**, 7298–7333.

5 E. Busseron, Y. Ruff, E. Moulin and N. Giuseppone, *Nanoscale*, 2013, **5**, 7098–7140.

6 X. M. Zhang, Q. D. Zeng and C. Wang, *Sci. China: Chem.*, 2014, **57**, 13–25.

7 L. Feng, T. Wang, Z. Tao, J. Huang, G. Li, Q. Xu, S. L. Tait and J. Zhu, *ACS Nano*, 2019, **13**, 10603–10611.

8 S. De Feyter, P. C. Grim, J. van Esch, R. M. Kellogg, B. L. Feringa and F. C. De Schryver, *J. Phys. Chem. B*, 1998, **102**, 8981–8987.

9 R. May, S. S. Jester and S. Höger, *J. Am. Chem. Soc.*, 2014, **136**, 16732–16735.

10 Z. Zhang, Y. Li, B. Song, Y. Zhang, X. Jiang, M. Wang, R. Tumbleson, C. Liu, P. Wang, X.-Q. Hao, T. Rojas, A. T. Ngo, J. L. Sessler, G. R. Newkome, S.-W. Hla and X. Li, *Nat. Chem.*, 2020, **12**, 468–474.

11 S. De Feyter and F. C. De Schryver, *J. Phys. Chem. B*, 2005, **109**, 4290–4302.

12 W. Mamdouh, H. Uji-i, J. S. Ladislaw, A. E. Dulcey, V. Percec, F. C. De Schryver and S. De Feyter, *J. Am. Chem. Soc.*, 2006, **128**, 317–325.

13 K. S. mali, J. Adisoejoso, E. Ghijsens, I. De Cat and S. De Feyter, *Acc. Chem. Res.*, 2012, **45**, 1309–1320.

14 U. Mazur and K. W. Hipps, *Chem. Commun.*, 2015, **51**, 4737–4749.

15 C. Ma, J. Li, S. Zhang, W. Duan and Q. Zeng, *Nanotechnology*, 2021, **32**, 382001.

16 S. Tan, J. Tao, W. Luo, H. Jiang, Y. Liu, H. Xu, Q. Zeng and H. Shi, *Chin. Chem. Lett.*, 2021, **32**, 1149–1152.

17 Y. Xiao, F. Cai, X. Peng, X. Kang, P. Lei, X. Li, H. Xu, X. Xunwen, T. Bin and Q. Zeng, *Chin. Chem. Lett.*, 2021, **32**, 3566–3569.

18 X. Peng, T. Meng, L. Wang, L. Cheng, W. Zhai, K. Deng, C.-Q. Ma and Q. Zeng, *Chin. Chem. Lett.*, 2023, **34**, 107568.

19 P. Lei, L. Ma, S. Zhang, J. Li, L. Gan, K. Deng, W. Duan, W. Li and Q. Zeng, *Chin. Chem. Lett.*, 2022, DOI: **10.1016/j.cclet.2022.108005**.

20 M. Lackinger and W. M. Heckl, *Langmuir*, 2009, **25**, 11307–11321.

21 X. Zhang, Q. Zeng and C. Wang, *RSC Adv.*, 2013, **3**, 11351–11366.

22 S. Q. Zhang, L. X. Cheng, Z. L. Gong, W. B. Duan, B. Tu, Y. W. Zhong and Q. D. Zeng, *Langmuir*, 2019, **35**, 6571–6577.

23 J. Li, X. Zu, Y. Qian, W. Duan, X. Xiao and Q. Zeng, *Chin. Chem. Lett.*, 2020, **31**, 10–18.

24 L. Ma, P. Wang, W. Duan, B. Tu and Q. Zeng, *Langmuir*, 2021, **37**, 11544–11551.

25 X. Li, J. Li, C. Ma, C. Chen, S. Zhang, B. Tu, W. Duan and Q. Zeng, *Chin. Chem. Lett.*, 2021, **32**, 1077–1080.

26 L. Ma, C. Ma, S. Zhang, J. Li, L. Gan, K. Deng, W. Duan, X. Li and Q. Zeng, *Langmuir*, 2022, **38**, 4434–4441.

27 S. Zhang, J. Zhang, K. Deng, J. Xie, W. Duan and Q. Zeng, *Phys. Chem. Chem. Phys.*, 2015, **17**, 24462–24467.

28 H. Dai, S. Wang, I. Hisaki, S. Nakagawa, N. Ikenaka, K. Deng, X. Xiao and Q. Zeng, *Chem. – Asian J.*, 2017, **12**, 2558–2564.

29 J. Gu, M. Wen, X. Liang, Z. Shi, M. V. Kirillova and A. M. Kirillov, *Crystals*, 2018, **8**, 83.

30 Q. Liang, Y. Yu, G. Feng, Y. Shen, L. Yang and S. Lei, *Chem. Commun.*, 2020, **56**, 12182–12185.

31 T. Meng, P. Lei, Y. Zhang, K. Deng, X. Xiao and Q. Zeng, *Chin. J. Chem.*, 2022, **40**, 2727–2733.

32 Q. Zhou, Y. Li, Q. Li, Y. Wang, Y. Yang, Y. Fang and C. Wang, *Nanoscale*, 2014, **6**, 8387–8391.

33 D. C. Y. Nguyen, L. Smykalla, T. N. H. Nguyen, T. Rüffer and M. Hietschold, *J. Phys. Chem. C*, 2016, **120**, 11027–11036.

34 J. Macleod, *J. Phys. D: Appl. Phys.*, 2019, **53**, 043002.

35 M. Li, K. Deng, S. B. Lei, Y. L. Yang, T. S. Wang, Y. T. Shen, C. R. Wang, Q. D. Zeng and C. Wang, *Angew. Chem., Int. Ed.*, 2008, **47**, 6717–6721.

36 X. Peng, L. Cheng, X. Zhu, Y. Geng, F. Zhao, K. Hu, X. Guo, K. Deng and Q. Zeng, *Nano Res.*, 2018, **11**, 5823–5834.

37 C. Ma, J. Li, S. Zhang, B. Liu, W. Duan, B. Tu, F. Zhao, X. Li and Q. Zeng, *J. Phys. Chem. C*, 2020, **124**, 23237–23242.

38 J. M. Macleod, Z. B. Chaouch, D. F. Perepichka and F. Rosei, *Langmuir*, 2013, **29**, 7318–7324.

39 Y. Xie, C. Liu, L. Cheng, Y. Fan, H. Li, W. Liu, L. Zhu, X. Li, K. Deng, Q. Zeng and S. Han, *Chin. Chem. Lett.*, 2022, **33**, 4649–4654.

40 M. Lackinger, S. Griessl, T. Markert, F. Jamitzky and W. M. Heckl, *J. Phys. Chem. B*, 2004, **108**, 13652–13655.

41 F. Silly, *J. Phys. Chem. C*, 2012, **116**, 10029–10032.

42 J. Li, B. Liu, W. Duan, B. Tu and Q. Zeng, *Surf. Sci.*, 2020, **700**, 121654.

43 J. Shi, Y. Li, X. Jiang, H. Yu, J. Li, H. Zhang, D. J. Trainer, S. W. Hla, H. Wang, M. Wang and X. Li, *J. Am. Chem. Soc.*, 2021, **143**, 1224–1234.

44 J. Fang, X. Zhu, W. Luo, J. Shi, L. Wang, L. Wang, B. Tu, Q. Zeng and X. Xiao, *Chin. Chem. Lett.*, 2022, **33**, 1100–1104.

45 C. N. Morrison, S. Ahn, J. K. Schnobrich and A. J. Matzger, *Langmuir*, 2011, **27**, 936–942.

46 J. Wang, L. M. Wang, C. Lu, H. J. Yan, S. X. Wang and D. Wang, *RSC Adv.*, 2019, **9**, 11659–11663.

47 S. Zhang, C. Chen, J. Li, C. Ma, X. Li, W. Ma, M. Zhang, F. Cheng, K. Deng and Q. Zeng, *Nanoscale*, 2022, **14**, 2419–2426.

48 J. Pang, F. Jiang, M. Wu, D. Yuan, K. Zhou, J. Qian, K. Su and M. Hong, *Chem. Commun.*, 2014, **50**, 2834–2836.

49 Y. Xie, H. Yang, Z. U. Wang, Y. Liu, H.-C. Zhou and J.-R. Li, *Chem. Commun.*, 2014, **50**, 563–565.

50 B. Delley, *J. Chem. Phys.*, 2000, **113**, 7756–7764.

51 J. P. Perdew and Y. Wang, *Phys. Rev. B: Condens. Matter Mater. Phys.*, 1992, **45**, 13244–13249.

52 J. P. Perdew, K. Burke and M. Ernzerhof, *Phys. Rev. Lett.*, 1996, **77**, 3865–3868.

This journal is © The Royal Society of Chemistry 2023